Beam-Helicity and Charge Asymmetries in the Bethe-Heitler and DVCS processes on an Unpolarised Proton Target
Paper Tag: PDVCS (v0.5)
Drafting Committee: DC90 (10 February 2011)

HERMES Collaboration

Abstract

Beam-helicity and charge asymmetries in the hard exclusive leptoproduction of real photons from an unpolarised proton target by a 27.6 GeV lepton beam are extracted from the HERMES unpolarised data set of 2006-2007 using a missing-mass event selection technique. The beam-charge asymmetry amplitudes extracted from the new data set are statistically more precise than those extracted from an earlier data set of 1996-2005 previously analysed in the same manner by the collaboration. Results from both data sets are found to be compatible with each other. Combined results from these data sets are extracted and are the statistically most precise asymmetry amplitude measurements available in the HERMES kinematic region.

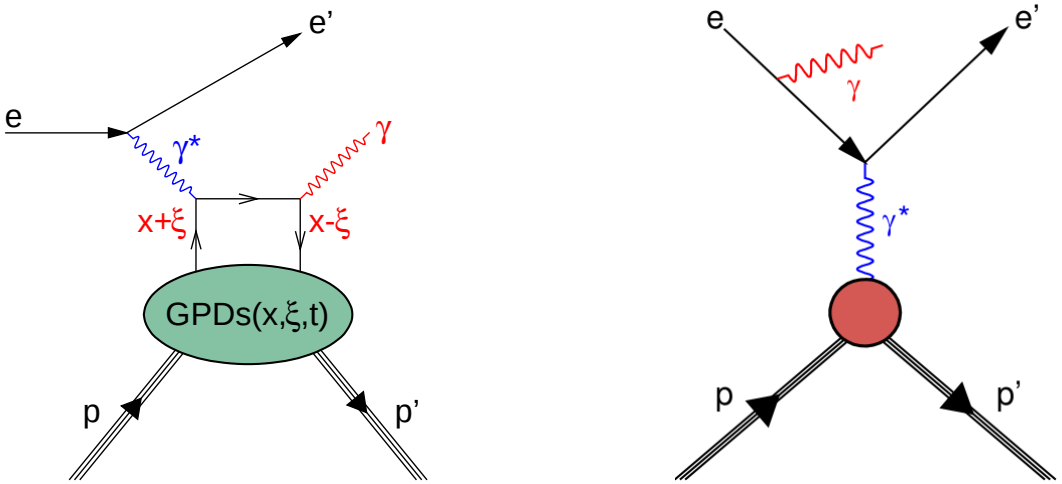

(a) DVCS (b) Bethe Heitler

Fig. 1. Left: The DVCS process in which an electron/positron (e, e')interacts with a quark in the nucleon (P) via a virtual photon γ^*). The quark is found in the nucleon with longitudinal momentum fraction $x + \xi$ and emits a real photon (γ). The quark is absorbed by the nucleon with fraction $x - \xi$. Right: The Bethe-Heitler process which has the same initial and final states as DVCS.

1 Introduction

Generalised Parton Distributions (GPDs) [?,?,?] encompass the familiar parton distribution functions (PDFs) and nucleon form factors to provide a comprehensive description of the structure of the nucleon. Although GPDs are difficult to access experimentally, the HERMES collaboration has previously published results [?,?,?,?,?] on the leptoproduction of real photons from a nucleon that can be used to constrain GPDs via Compton Form Factors (CFFs). Each CFF is a convolution of a hard scattering kernel with a GPD that describes a soft part of the scattering process.

Generalised parton distributions depend upon four kinematic variables: the Mandelstam variable $t = (p-p')^2$, which is the squared momentum transfer to the target nucleon in the scattering process with p (p') representing the initial (final) four momentum of the proton; the average fraction x of the nucleon's longitudinal momentum carried by the active quark throughout the scattering process; half the difference in the change of the fraction of the nucleon's longitudinal momentum carried by the active quark at the start and end of the process, written as the skewness variable ξ; and the square $-Q^2 = q^2$ of the exchanged virtual photon's four-momentum q. In the Bjorken limit of $Q^2 \to \infty$ with fixed t, ξ is related to the Bjorken variable $x_B = \frac{-q^2}{2p.q}$ as $\xi \approx \frac{x_B}{2-x_B}$. The results are presented against x_B because there is no consensus on an experimentally observable representation of ξ.

Leptoproduction of real photons $(ep \to ep\gamma)$ can be described in terms of the two experimentally indistinguishable processes shown in Fig. 1: the Deeply Virtual Compton Scattering (DVCS) process, which is the emission of a real photon by a quark from the nucleon, and the Bethe-Heitler (BH) process, which is elastic lepton-proton scattering with the emission of a

Bremsstrahlung photon by the lepton. The BH process is calculable in the QED framework; this process is dominant at the kinematic conditions of the HERMES experiment, but the scattering amplitudes of the two processes interfere and the large BH amplitude amplifies the contribution of the DVCS amplitude to the interference term. It is through the study of this interference term at HERMES that useful information for the constraint of certain GPDs can be obtained.

The differential four-fold cross section for the leptoproduction of real photons from an unpolarised target can be written [**?**]

$$\frac{\mathrm{d}^4\sigma}{\mathrm{d}x_\mathrm{B}\mathrm{d}Q^2\mathrm{d}|t|\mathrm{d}\phi} = \frac{x_\mathrm{B}e^6}{32(2\pi)^4Q^4\sqrt{1+\epsilon^2}}|\tau|^2, \tag{1}$$

where e is the elementary charge, $\epsilon = 2x_\mathrm{B}\frac{M}{Q}$ with M the nucleon mass and ϕ is the azimuthal angle between the scattering and production planes REF_TRENTO. The scattering amplitude τ can be written

$$|\tau|^2 = |\tau_\mathrm{BH}|^2 + |\tau_\mathrm{DVCS}|^2 + \mathrm{I}, \tag{2}$$

with contributions from the BH process (τ_BH), the DVCS process (τ_DVCS) and the interference term (I). These contributions can be written

$$|\tau_\mathrm{BH}|^2 = \frac{K_\mathrm{BH}}{\mathcal{P}_1(\phi)\mathcal{P}_2(\phi)}\left(c_0^\mathrm{BH} + \sum_{n=1}^{2} c_n^\mathrm{BH}\cos(n\phi)\right), \tag{3}$$

$$|\tau_\mathrm{DVCS}|^2 = K_\mathrm{DVCS}\left(c_0^\mathrm{DVCS} + \sum_{n=1}^{2} c_n^\mathrm{DVCS}\cos(n\phi) + \lambda s_1^\mathrm{DVCS}\sin\phi\right), \tag{4}$$

$$\mathrm{I} = \frac{-e_\ell K_\mathrm{I}}{\mathcal{P}_1(\phi)\mathcal{P}_2(\phi)}\left(c_0^\mathrm{I} + \sum_{n=1}^{3} c_n^\mathrm{I}\cos(n\phi) + \lambda\sum_{n=1}^{2} s_n^\mathrm{I}\sin(n\phi)\right), \tag{5}$$

where $\mathcal{P}_1(\phi)$ and $\mathcal{P}_2(\phi)$ are the lepton propagators of the BH process and λ and e_ℓ are respectively the helicity and unit charge of the lepton beam. The quantities $K_\mathrm{BH} = 1/(x_\mathrm{B}^2 t(1+\epsilon^2)^2)$, $K_\mathrm{DVCS} = 1/Q^2$ and $K_\mathrm{I} = 1/(x_\mathrm{B}yt)$ are kinematic factors, where y is the fraction of the beam energy carried by the virtual photon in the target rest frame. A full explanation of the Fourier coefficients $[c_n^V, s_n^W]$ ($V \in [\mathrm{BH,DVCS,I}]$ and $W \in [\mathrm{DVCS,I}]$) can be found in Ref. [**?**].

This paper provides a set of results analogous to those reported in Ref. [**?**]. The analysis presented here additionally includes a larger, independent data set taken during the years 2006 and 2007 after the experiment was upgraded in the target region. The results in this paper do not make use of any of the information from the upgraded detector equipment (i.e. uses a missing-mass technique for event selection), but represent the largest DVCS data set that will

be published by HERMES. For more details on the physics implications and general experimental technique, the reader is referred to Ref. [**?**].

There are two sets of asymmetries that are measured at HERMES with an unpolarised target and a polarised electron or positron beam: beam-helicity asymmetries and beam-charge asymmetries. It is possible to disentangle the DVCS and interference contributions to the beam-helicity asymmetry due to the beam-charge dependence of the interference term, so that this paper, as Ref. [**?**], presents results on the following asymmetries:

$$\begin{aligned}\mathcal{A}_{\mathrm{LU}}^{\mathrm{I}}(\phi) &\equiv \frac{(\mathrm{d}\sigma(\phi)^{+\rightarrow} - \mathrm{d}\sigma(\phi)^{+\leftarrow}) - (\mathrm{d}\sigma(\phi)^{-\rightarrow} - \mathrm{d}\sigma(\phi)^{-\leftarrow})}{(\mathrm{d}\sigma(\phi)^{+\rightarrow} + \mathrm{d}\sigma(\phi)^{+\leftarrow}) + (\mathrm{d}\sigma(\phi)^{-\rightarrow} + \mathrm{d}\sigma(\phi)^{-\leftarrow})} \\ &= \frac{-\dfrac{K_{\mathrm{I}}}{\mathcal{P}_1(\phi)\mathcal{P}_2(\phi)} \displaystyle\sum_{n=1}^{2} s_n^{\mathrm{I}} \sin(n\phi)}{\dfrac{K_{\mathrm{BH}}}{\mathcal{P}_1(\phi)\mathcal{P}_2(\phi)} \displaystyle\sum_{n=0}^{2} c_n^{\mathrm{BH}} \cos(n\phi) + K_{\mathrm{DVCS}} \sum_{n=0}^{2} c_n^{\mathrm{DVCS}} \cos(n\phi)},\end{aligned} \tag{6}$$

$$\begin{aligned}\mathcal{A}_{\mathrm{LU}}^{\mathrm{DVCS}}(\phi) &\equiv \frac{(\mathrm{d}\sigma(\phi)^{+\rightarrow} + \mathrm{d}\sigma(\phi)^{-\rightarrow}) - (\mathrm{d}\sigma(\phi)^{+\leftarrow} + \mathrm{d}\sigma(\phi)^{-\leftarrow})}{(\mathrm{d}\sigma(\phi)^{+\rightarrow} + \mathrm{d}\sigma(\phi)^{-\rightarrow}) + (\mathrm{d}\sigma(\phi)^{+\leftarrow} + \mathrm{d}\sigma(\phi)^{-\leftarrow})} \\ &= \frac{K_{\mathrm{DVCS}} s_1^{\mathrm{DVCS}} \sin\phi}{\dfrac{K_{\mathrm{BH}}}{\mathcal{P}_1(\phi)\mathcal{P}_2(\phi)} \displaystyle\sum_{n=0}^{2} c_n^{\mathrm{BH}} \cos(n\phi) + K_{\mathrm{DVCS}} \sum_{n=0}^{2} c_n^{\mathrm{DVCS}} \cos(n\phi)},\end{aligned} \tag{7}$$

$$\begin{aligned}\mathcal{A}_{\mathrm{C}}(\phi) &\equiv \frac{(\mathrm{d}\sigma(\phi)^{+\rightarrow} + \mathrm{d}\sigma(\phi)^{+\leftarrow}) - (\mathrm{d}\sigma(\phi)^{-\rightarrow} + \mathrm{d}\sigma(\phi)^{-\leftarrow})}{(\mathrm{d}\sigma(\phi)^{+\rightarrow} + \mathrm{d}\sigma(\phi)^{+\leftarrow}) + (\mathrm{d}\sigma(\phi)^{-\rightarrow} + \mathrm{d}\sigma(\phi)^{-\leftarrow})} \\ &= \frac{-\dfrac{K_{\mathrm{I}}}{\mathcal{P}_1(\phi)\mathcal{P}_2(\phi)} \displaystyle\sum_{n=0}^{3} c_n^{\mathrm{I}} \cos(n\phi)}{\dfrac{K_{\mathrm{BH}}}{\mathcal{P}_1(\phi)\mathcal{P}_2(\phi)} \displaystyle\sum_{n=0}^{2} c_n^{\mathrm{BH}} \cos(n\phi) + K_{\mathrm{DVCS}} \sum_{n=0}^{2} c_n^{\mathrm{DVCS}} \cos(n\phi)},\end{aligned} \tag{8}$$

where $\mathrm{d}\sigma(\phi)^{+}$ ($\mathrm{d}\sigma(\phi)^{-}$) refers to cross sections with positive (negative) beam charge and $\mathrm{d}\sigma(\phi)^{\rightarrow}$ ($\mathrm{d}\sigma(\phi)^{\leftarrow}$) refer to cross sections taken with beam spin parallel and anti-parallel with the beam momentum.

2 Experiment and Data Selection

The data were collected in 2006 and 2007 with the HERMES spectrometer [?] using the longitudinally polarised 27.6 GeV electron and positron beams incident upon an unpolarised hydrogen gas target internal to the HERA lepton storage ring at DESY. The integrated luminosities of the electron and positron data samples respectively are approximately $246\,\mathrm{pb}^{-1}$ and $1460\,\mathrm{pb}^{-1}$, with average beam polarisations of 30.3 % and 39.2% [?]. The procedure used to select events is identical to that used in Ref. [?]. A brief summary of this procedure is outlined in the following; consult Refs. [?,?] for more details. An event was selected as having exactly one photon and one lepton track detected within the acceptance of the spectrometer.

The event selection is subject to the kinematic constraints $1\,\mathrm{GeV}^2 < \mathrm{Q}^2 < 10\,\mathrm{GeV}^2$, $0.03 < x_\mathrm{B} < 0.35$, $W^2 > 9\,\mathrm{GeV}^2$ and $\nu < 22\,\mathrm{GeV}$, where W is the invariant mass of the $\gamma^* p$ system and ν is the energy of the virtual photon in the target rest frame. The polar angle between the virtual and real photons was required to be within the limits 5 mrad $< \theta_{\gamma^*\gamma} <$ 45 mrad.

An "exclusive" event sample was selected using a missing-mass technique requiring that the squared missing-mass $M_\mathrm{X}^2 = (q + p - q')^2$ of the $ep \to e\gamma\mathrm{X}$ measurement corresponded to the square of the proton mass within the limits of the energy resolution of the calorimeter. Here, q is the four-momentum of the virtual photon that mediates the lepton-proton scattering process, p is the four-momentum of the target proton and q' is the four momentum of the produced photon. The "exclusive region" was defined as $(-1.5\,\mathrm{GeV})^2 < M_\mathrm{X}^2 < (1.7\,\mathrm{GeV})^2$, as in Ref. [?]. This exclusive region was shifted by up to $0.17\,\mathrm{GeV}^2$ to reflect observed differences in the distributions of the electron and positron data samples and to account for the time dependence of the missing-mass distributions observed in the 2007 dataset [?].

3 Experimental Extraction of Asymmetry Amplitudes

The expectation value of the experimental yield N is parameterised as

$$\langle N(e_\ell, P_\ell, \phi)\rangle = \mathcal{L}(e_\ell, P_\ell)\eta(e_\ell, \phi)\mathrm{d}\sigma_{UU}(\phi) \times [1 + P_\ell \mathcal{A}_\mathrm{LU}^\mathrm{DVCS}(\phi) + e_\ell P_\ell \mathcal{A}_\mathrm{LU}^\mathrm{I}(\phi) + e_\ell \mathcal{A}_\mathrm{C}(\phi)], \quad (9)$$

where $\mathcal{L}$ is the integrated luminosity, η the detection efficiency and $\mathrm{d}\sigma_{UU}$ denotes the cross section for an unpolarised target integrated over both beam charges and beam helicities. The asymmetries $\mathcal{A}_\mathrm{LU}^\mathrm{I}(\phi)$, $\mathcal{A}_\mathrm{LU}^\mathrm{DVCS}(\phi)$ and $\mathcal{A}_\mathrm{C}(\phi)$ are expanded in ϕ as

$$\mathcal{A}_\mathrm{LU}^\mathrm{I}(\phi) \simeq \sum_{n=1}^{2} A_\mathrm{LU,I}^{\sin(n\phi)} \sin(n\phi) + \sum_{n=0}^{1} A_\mathrm{LU,I}^{\cos(n\phi)} \cos(n\phi), \quad (10)$$

$$\mathcal{A}_\mathrm{LU}^\mathrm{DVCS}(\phi) \simeq \sum_{n=1}^{2} A_\mathrm{LU,DVCS}^{\sin(n\phi)} \sin(n\phi) + \sum_{n=0}^{1} A_\mathrm{LU,DVCS}^{\cos(n\phi)} \cos(n\phi), \quad (11)$$

$$\mathcal{A}_{\mathrm{C}}(\phi) \simeq \sum_{n=0}^{3} A_{\mathrm{C}}^{\cos(n\phi)} \cos(n\phi) + A_{\mathrm{C}}^{\sin\phi} \sin\phi, \tag{12}$$

where the approximation is due to the truncation of the infinite Fourier series caused by the azimuthal dependencies in the denominators from Eqs. 6-8. Only the $\sin(n\phi)$ terms of the $\mathcal{A}_{\mathrm{LU}}$ asymmetries and the $\cos(n\phi)$ terms of the $\mathcal{A}_{\mathrm{C}}$ asymmetry are physically motivated. The other terms are included as both a consistency check for extraneous harmonics caused by the denominators in Eqs. 6-8 and as a test of the normalisation of the fit. These terms are expected to be small.

A maximum-likelihood fitting technique [**?**] was used to extract the asymmetry amplitudes in each kinematic bin of $-t$, x_{B} and Q^2. This method, described in Ref. [**?**], fits the expected azimuthal distribution function to the data without introducing binning effects in ϕ. Weights are introduced per event in the fitting procedure to account for luminosity imbalances with respect to the beam charge and polarisation.

The asymmetry amplitudes $A_{\mathrm{LU,I/DVCS}}^{\sin(n\phi)}$ and $A_{\mathrm{C}}^{\cos(n\phi)}$ relate respectively to the Fourier coefficients s_n^W and c_n^V from the interference and DVCS terms in Eqs. 6-8. The asymmetry amplitudes may also be affected by the lepton progopagators and the other ϕ-dependent terms in the denominators in Eqs. 6-8. The s_n^W and c_n^V Fourier coefficients are depend on "$\mathcal{C}$-functions", each of which $\mathcal{C}$-function is a combination of complex Compton Form Factors. A CFF is a convolution of a GPD with a hard scattering kernel. Contributions of GPDs to the cross section may ne relatively suppressed by powers of $1/Q$, the origin of which may be kinematic in nature or due to the twist level of the GPD. The access from each asymmetry amplitude to a GPD is called twist-n depending upon the part of the twist-decomposed cross-section in which the amplitude appears. Leading twist is twist-2. Typically, the contribution of a twist-n GPD, and hence the corresponding CFF, is suppressed by $\mathcal{O}(1/Q^{n-2})$. Table 1 presents the asymmetry amplitudes extracted in this analysis and the related Fourier coefficients, dominant $\mathcal{C}$-function, twist-level and levels of suppression.

At HERMES kinematic conditions, the leading-twist beam-helicity asymmetry amplitude is $A_{\mathrm{LU,I}}^{\sin\phi}$ and the leading beam-charge asymmetry amplitude is $A_{\mathrm{C}}^{\cos\phi}$. These asymmetry amplitudes for an unpolarised target are sensitive respectively to Fourier coefficients $s_{1,\mathrm{unp}}^{\mathrm{I}}$ and $c_{1,\mathrm{unp}}^{\mathrm{I}}$. Both of these Fourier coefficients have a dominant contribution from the $\mathcal{C}_{\mathrm{unp}}^{\mathrm{I}}$-function:

$$s_{1,\mathrm{unp}}^{\mathrm{I}} \approx 8\lambda k y(2-y)\mathfrak{Im}\mathcal{C}_{\mathrm{unp}}^{\mathrm{I}}, \tag{13}$$

$$c_{1,\mathrm{unp}}^{\mathrm{I}} \approx 8k(2-2y+y^2)\mathfrak{Re}\mathcal{C}_{\mathrm{unp}}^{\mathrm{I}}, \tag{14}$$

where the kinematic factor $k \propto \sqrt{-t}/Q$ originates from the BH propagators. The $\mathcal{C}_{\mathrm{unp}}^{\mathrm{I}}$-function

can be written [?]

$$\mathcal{C}^{\mathrm{I}}_{\mathrm{unp}} = F_1\mathcal{H} + \frac{x_{\mathrm{B}}}{2-x_{\mathrm{B}}}(F_1+F_2)\widetilde{\mathcal{H}} - \frac{t}{4M^2}F_2\mathcal{E}, \tag{15}$$

where F_1 and F_2 are respectively the Dirac and Pauli form factors of the nucleon and $\mathcal{H}$, $\widetilde{\mathcal{H}}$ and $\mathcal{E}$ are CFFs that relate respectively to the GPDs H, $\widetilde{H}$ and E. At HERMES kinematic conditions (where x_{B} and $\frac{t}{4M^2}$ are of order 0.1), to first approximation the contributions of CFFs $\widetilde{\mathcal{H}}$ and $\mathcal{E}$ can be neglected in Eq. 15 with respect to $\mathcal{H}$ since they are kinematically suppressed by an order of magnitude or more. Hence, in this approximation, the behaviour of $\mathcal{C}^{\mathrm{I}}_{\mathrm{unp}}$ is determined by CFF $\mathcal{H}$ and therefore GPD H. Using this dependence, H can be constrained through measurements of $A^{\sin\phi}_{\mathrm{LU,I}}$ and $A^{\cos\phi}_{\mathrm{C}}$. The asymmetry amplitudes $A^{\sin(2\phi)}_{\mathrm{LU,I}}$, $A^{\cos(0\phi)}_{\mathrm{C}}$ and $A^{\cos(2\phi)}_{\mathrm{C}}$ also depend upon this $\mathcal{C}$-function. However, the $A^{\cos(0\phi)}_{\mathrm{C}}$ amplitude is kinematically suppressed compared to the $A^{\cos\phi}_{\mathrm{C}}$ amplitude, whereas the $A^{\sin(2\phi)}_{\mathrm{LU,I}}$ and $A^{\cos(2\phi)}_{\mathrm{C}}$ amplitudes enter the cross section at a higher twist level (see Table 1).

The DVCS asymmetry amplitude $A^{\sin\phi}_{\mathrm{LU,DVCS}}$ has a dominant contribution from the $\mathcal{C}^{\mathrm{DVCS}}_{\mathrm{unp}}$ function, which is bilinear in CFFs. However, the amplitude is suppressed by the larger BH contribution in the denominator of Eq. 7. As a result of the more complicated dependence on the CFFs and this suppression, it will be more difficult to extract useful information for the constraint of GPDs from the measurement of $A^{\sin\phi}_{\mathrm{LU,DVCS}}$ than from the kinematically-unsuppressed leading-twist amplitudes.

The $A^{\cos(3\phi)}_{\mathrm{C}}$ amplitude depends on the $c^{\mathrm{I}}_{3,\mathrm{unp}}$ Fourier coefficient and hence the $\mathcal{C}^{\mathrm{I}}_{\mathrm{T,unp}}$ function. This $\mathcal{C}$-function receives contributions from both the BH and DVCS processes and therefore depends on F_1, F_2 and CFFs. Although the CFFs in this function are of leading twist, they relate to gluon helicity-flip GPDs and are thus suppressed by α_{S}/π.

Asymmetry Amplitude	Fourier Coefficient	Dominant CFF Dependence	Twist Level	Suppression
$A^{\sin\phi}_{\mathrm{LU,I}}$	$s^{\mathrm{I}}_{1,\mathrm{unp}}$	$\mathfrak{Im}\mathcal{C}^{\mathrm{I}}_{\mathrm{unp}}$	2	$n=2$
$A^{\sin(2\phi)}_{\mathrm{LU,I}}$	$s^{\mathrm{I}}_{2,\mathrm{unp}}$	$\mathfrak{Im}\mathcal{C}^{\mathrm{I}}_{\mathrm{unp}}$	3	$n=3$
$A^{\sin\phi}_{\mathrm{LU,DVCS}}$	$s^{\mathrm{DVCS}}_{1,\mathrm{unp}}$	$\mathfrak{Im}\mathcal{C}^{\mathrm{DVCS}}_{\mathrm{unp}}$	3	$n=3$
$A^{\cos(0\phi)}_{\mathrm{C}}$	$c^{\mathrm{I}}_{0,\mathrm{unp}}$	$\mathfrak{Re}\mathcal{C}^{\mathrm{I}}_{\mathrm{unp}}$	2	$n=2$
$A^{\cos\phi}_{\mathrm{C}}$	$c^{\mathrm{I}}_{1,\mathrm{unp}}$	$\mathfrak{Re}\mathcal{C}^{\mathrm{I}}_{\mathrm{unp}}$	2	$n=2$
$A^{\cos(2\phi)}_{\mathrm{C}}$	$c^{\mathrm{I}}_{2,\mathrm{unp}}$	$\mathfrak{Re}\mathcal{C}^{\mathrm{I}}_{\mathrm{unp}}$	3	$n=3$
$A^{\cos(3\phi)}_{\mathrm{C}}$	$c^{\mathrm{I}}_{3,\mathrm{unp}}$	$\mathfrak{Re}\mathcal{C}^{\mathrm{I}}_{\mathrm{T,unp}}$	2	$n=2$, α_{S}/π

Table 1
Asymmetry amplitudes that can be extracted from the available data set, the related Fourier coefficients, the $\mathcal{C}$-functions, the twist level and the suppression at HERMES kinematic conditions [?].

4 Background Corrections and Systematic Uncertainties

The extracted asymmetry amplitudes are subject to systematic uncertainties that result from a combination of background processes, year-dependent shifts in the missing-mass event distributions and various detector and binning effects determined as in Refs. [?,?]. The 1996-2005 data sample also has a systematic uncertainty from misalignment of the spectrometer, which was eliminated for the 2006-2007 data sample. Contributions to the uncertainties on the amplitude measurements arise from background in the data from events that include neutral meson production. The procedure is described in detail in Refs. [?,?] and the contributions to the uncertainties of the measurements addressed here are given in Table 2. The largest contamination in the data sample is expected to come from the excitation of a target proton to a Δ^+ resonance. The separation of these events from the elastic sample is nto feasible because the recoiling proton is not detected. No systematic uncertainty is assigned for the contribution from these events; they are treated as part of the signal. A Monte Carlo calculation based on the parameterisation of Ref. [?] is used to estimate the contribution to the event sample from resonant production in each kinematic bin. The results, denoted associated fraction and labelled "assoc. fraction", are shown in the last row of each figure in the results section. The method used to perform the estimation is described in detail in Ref. [?].

Another contribution to the systematic uncertainty comes from the relative shift of the missing-mass distributions between the electron and positron data samples [?,?]. The exclusive region in the missing-mass distribution is adjusted for each calorimeter calibration period for data collected in 2007 to account for the observed time dependence. One quarter of the difference between the asymmetries extracted using the standard and shifted missing-mass windows is taken as the corresponding systematic uncertainty. The beam polarisation measurement has a total uncertainty of 2.8% and 3.4% for the 1996-2005 and 2006-2007 data taking periods respectively, which is present in the beam-helicity amplitudes and is quoted as an independent scale uncertainty.

The predominant contribution to the systematic uncertainty arises from detector effects, including the acceptance of the spectrometer, smearing effects due to detector resolution and radiative processes, and finite bin width in $-t$, $x_{\rm B}$ and Q^2. In order to quantify these effects, DVCS/BH events were generated using a Monte Carlo simulation of the spectrometer that included these effects. The simulation used an event generator based on the GPD model described in Ref. [?] because it describes the data well and to keep consistency with Ref. [?]. Asymmetry amplitudes were extracted from these simulated events using the same analysis procedure used to extract amplitudes from experimental data. In each kinematic bin, the systematic uncertainty was determined as the difference between the asymmetry amplitude reconstructed from the simulated DVCS/BH data and that calculated from the same GPD model at the average $-t$, $x_{\rm B}$ and Q^2 value for that bin. The total systematic uncertainty for the 2006-2007 data sample was determined for each kinematic bin from the uncertainty contributions of the background corrections, detector effects and missing-mass shift uncertainties added in quadrature. These contributions are summarised in Table 2.

	Background	Missing-Mass Shift	Detector Effects		Total
$A_{\mathrm{LU,I}}^{\sin\phi}$	0.005	0.005	0.025		0.026
$A_{\mathrm{LU,I}}^{\sin(2\phi)}$	0.005	0.001	0.002		0.006
$A_{\mathrm{LU,DVCS}}^{\sin\phi}$	0.004	0.007	0.001		0.008
$A_{\mathrm{C}}^{\cos(0\phi)}$	0.001	0.004	0.007		0.008
$A_{\mathrm{C}}^{\cos\phi}$	0.002	0.001	0.002		0.003
$A_{\mathrm{C}}^{\cos(2\phi)}$	0.001	0.001	0.001		0.002
$A_{\mathrm{C}}^{\cos(3\phi)}$	0.000	0.001	0.001		0.001

Table 2
The contributions to systematic uncertainty due to the background correction, the time-dependence of the missing-mass distributions and detector effects for the 2006-2007 data to the total systematic uncertainty. The total systematic uncertainties, shown in the right-most column, are the individual contributions added in quadrature.

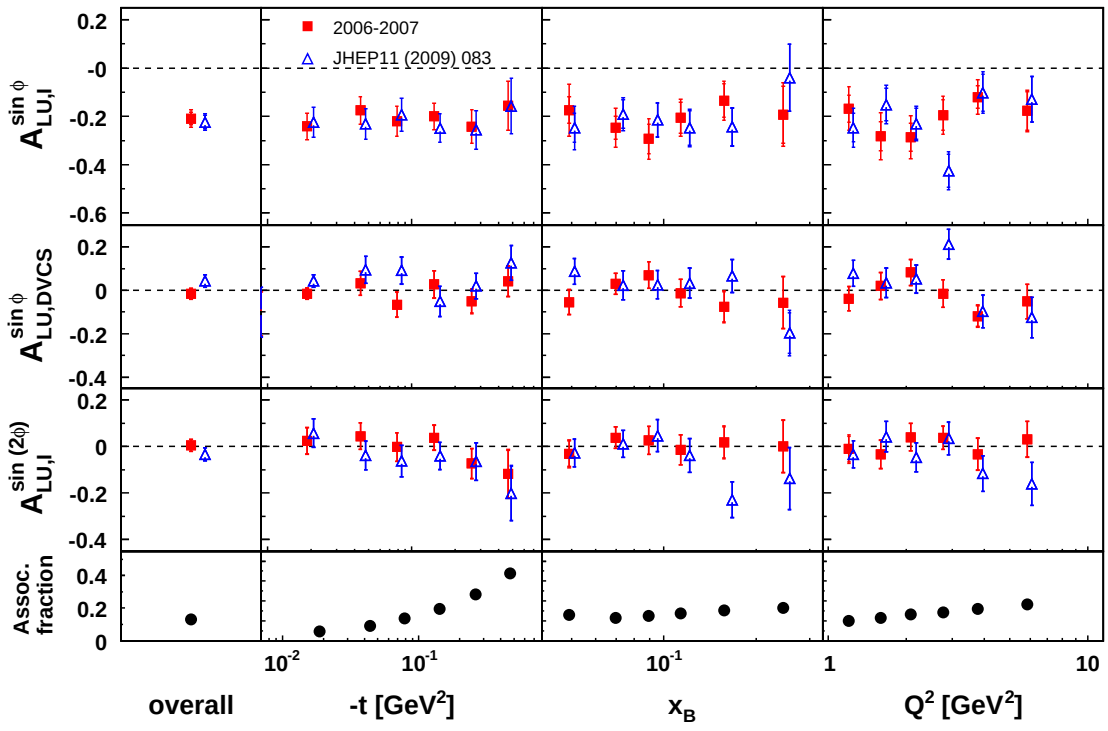

Fig. 2. Beam-helicity asymmetry amplitudes extracted separately from the 1996-2005 (open triangles) and 2006-2007 (filled squares) hydrogen data. An additional 2.8 % and 3.4 % scale uncertainty for the 1996-2005 and 2006-2007 data respectively is present in the amplitudes due to the imprecision of the beam polarisation measurement. The inner error bars represent the statistical uncertainties, while total error bars denote the statistical and systematic uncertainties added in quadrature. The simulated fractional contribution from associated production to the yield in each kinematic bin is shown in the bottom row.

5 Results

Results for the beam-helicity and beam-charge asymmetry amplitudes extracted separately from previously published 1996-2005 [**?**] and the new 2006-2007 hydrogen data sets, are presented in Figs. 2 and 3. The asymmetry amplitudes extracted from the combined 1996-2007 hydrogen data set are shown in Figs. 4 and 5. Each of the asymmetry amplitudes is shown extracted in one bin over all kinematic variables ("overall") and also projected against $-t$, x_B and Q^2. All of the extracted asymmetry amplitudes are subject to a fractional contribution to the event yield from associated production ("assoc. fraction"), which is shown in the bottom row of each figure. The beam-helicity asymmetry amplitudes are subject to an additional scale uncertainty from the measurement of the beam polarisation, which is stated in the captions of the figures. A statistical test was applied in order to check for possible incompatiability between the asymmetry amplitudes extracted from both data sets. Only the statistical uncertainties were employed in this test. The results show that the the two data sets are not incompatible. The $A_{LU,I}$, $A_{LU,DVCS}$ and A_C asymmetry amplitudes can therefore be extracted from the complete hydrogen data set recorded during the entire experimental operation of HERMES.

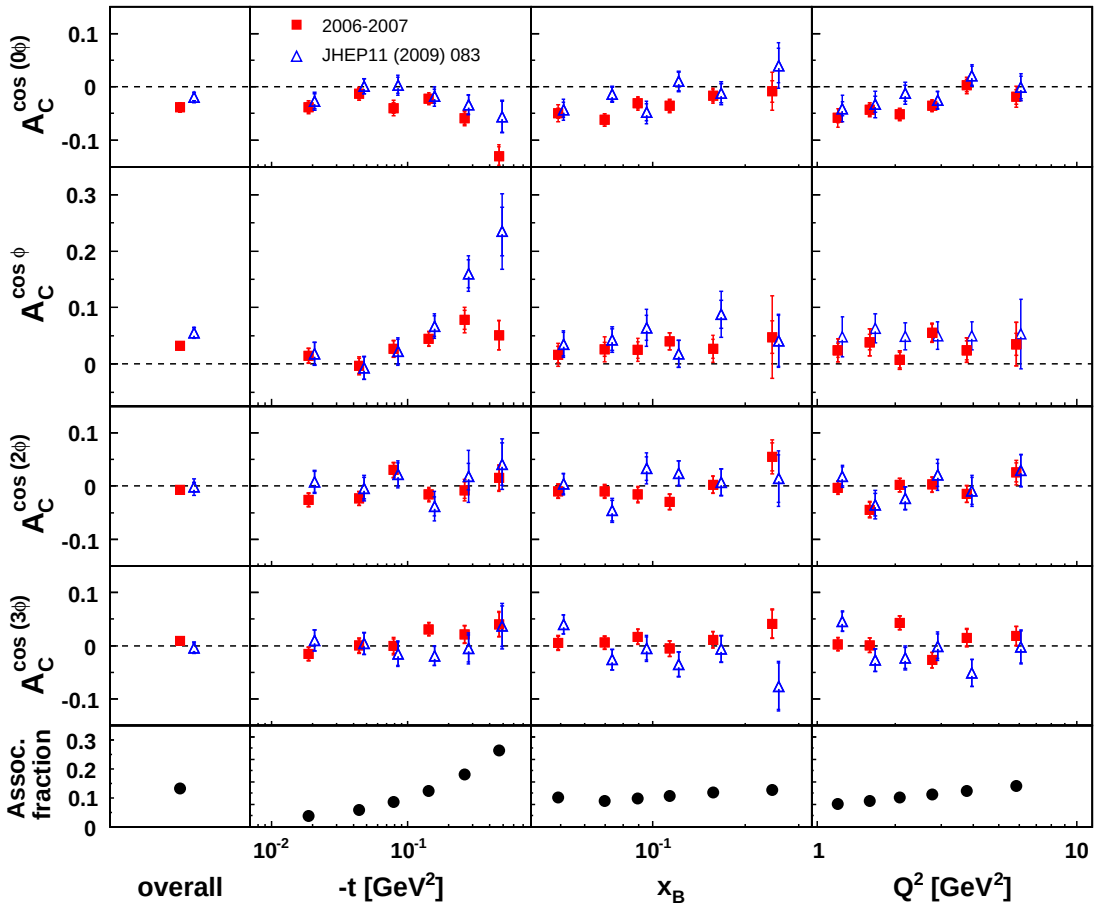

Fig. 3. Beam-charge asymmetry amplitudes extracted separately from the 1996-2005 (open triangles) and 2006-2007 (filled squares) hydrogen data. The inner error bars represent the statistical uncertainties, while the total error bars denote the statistical and systematic uncertainties added in quadrature. The simulated fractional contribution from associated production to the yield in each kinematic bin is shown in the bottom row.

The results of the beam-helicity and beam-charge asymmetry amplitudes extracted from the complete 1996-2007 hydrogen sample are shown in Figs. 4 and 5. The number of analysable DVCS/BH events available from the 2006-2007 data set (XXXXX) is approximately three times greater than the number events recorded in the 1996-2005 sample (XXXX). The asymmetry amplitudes extracted from the complete 1996-2007 data set are thus weighted towards the 2006-2007 result. This is most noticeable in the set of beam-charge asymmetry amplitudes because the beam polarisation was lower in 2006 and 2007.

The first and second harmonics of $\mathcal{A}_{\mathrm{LU,I}}$, which are sensitive to the interference term in the scattering amplitude, are shown in the first and third rows of Fig. 4. The leading-twist amplitude $A_{\mathrm{LU,I}}^{\sin\phi}$ has the largest value of any of the amplitudes when extracted in a single bin from the entire data set. This amplitude has no strong dependence on $-t$, x_{B} or Q^2, implying a strong dependence at smaller values of $-t$ as the amplitude must diminish at low t values due to the dependence of the amplitude on the factor k from in Eq. 13. The $A_{\mathrm{LU,I}}^{\sin\phi}$ amplitude is sensitive to the imaginary part of the CFF $\mathcal{H}$ and thereby can constrain GPD H. The twist-3

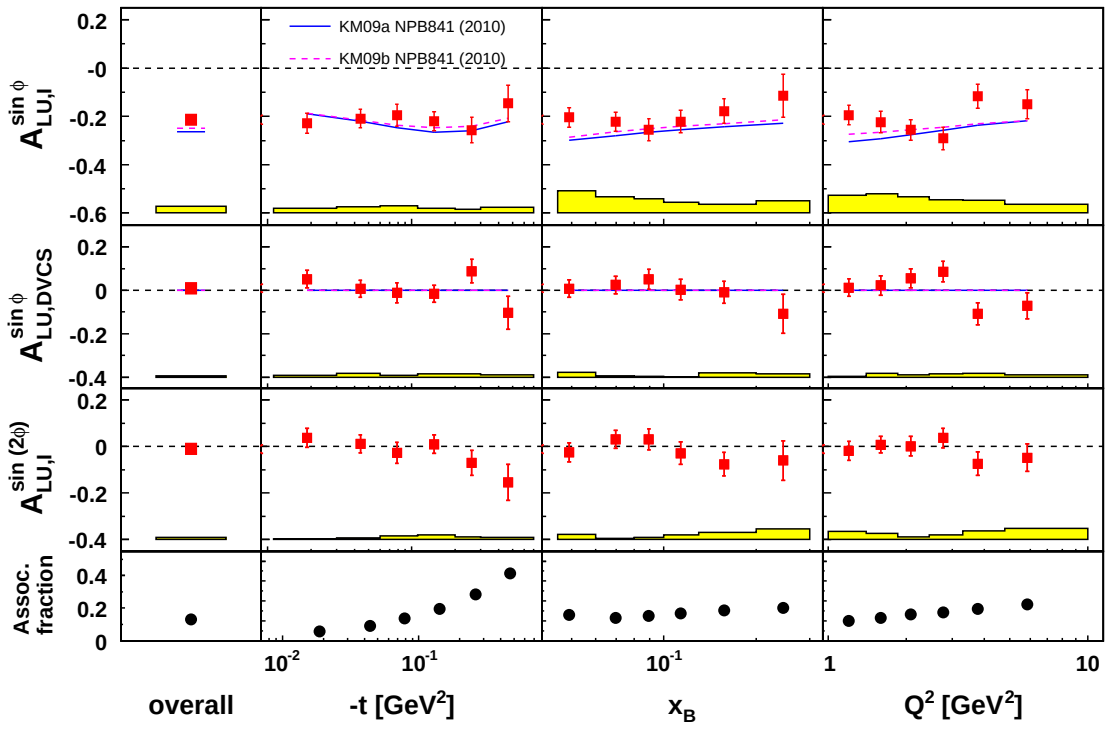

Fig. 4. The $A_{\mathrm{LU,I}}^{\sin\phi}$, $A_{\mathrm{LU,DVCS}}^{\sin\phi}$ and $A_{\mathrm{LU,I}}^{\sin(2\phi)}$ beam-helicity amplitudes extracted from all the hydrogen data recorded at HERMES from 1996 until 2007. The error bars (bands) represent the statistical (systematic) uncertainties. Theoretical calculations from the model described in [**?**] are shown as solid and dashed lines. See text for details. The simulated fractional contribution from associated production to the yield in each kinematic bin is shown in the bottom row.

$A_{\mathrm{LU,I}}^{\sin(2\phi)}$ amplitudes are compatible with zero, as are the twist-3 $A_{\mathrm{LU,DVCS}}^{\sin\phi}$ amplitudes dependent on the squared DVCS term. These are shown in the second row of Fig. 4. Neither of these amplitudes show any clear dependence on $-t$, x_{B} or Q^2. The systematic error bands of the asymmetry amplitudes extracted from the combined data set were determined using Monte Carlo simulations that reflect the equipment used used in the various stages of the HERMES experiment.

The $A_{\mathrm{C}}^{\cos(n\phi)}$ amplitudes are shown in Fig. 5. The leading-twist $A_{\mathrm{C}}^{\cos(0\phi)}$ and $A_{\mathrm{C}}^{\cos\phi}$ amplitudes are both non-zero. There is a relationship between $A_{\mathrm{C}}^{\cos(0\phi)}$ and $A_{\mathrm{C}}^{\cos\phi}$ as the Fourier coefficient $c_{0,\mathrm{UNP}}^{\mathrm{I}}$ is inversely proportional to $c_{1,\mathrm{UNP}}^{\mathrm{I}}$ via the kinematic factor k introduced in Eq 14. These amplitudes diverge with opposite sign from zero at increasing values of $-t$ but they have no discernible dependence on x_{B} and Q^2. The $A_{\mathrm{C}}^{\cos(2\phi)}$ and $A_{\mathrm{C}}^{\cos(3\phi)}$ amplitudes are both consistent with zero and have no significant variation in value over the range in $-t$, x_{B} and Q^2. The amplitude $A_{C}^{\cos(2\phi)}$ is related to twist-3 GPDs and $A_{\mathrm{C}}^{\cos(3\phi)}$ relates to gluon helicity-flip GPDs. Both of these amplitudes are expected to be suppressed at HERMES kinematic conditions compared to the leading twist amplitudes.

The curves in Figs. 4 and 5 show calculations from a global fit of GPDs to experimental data[**?**]. The basic model is based on a minimalist dual representation of GPDs with only (very) weakly entangled skewedness and t dependences. In the model, the t dependence is approximated by a

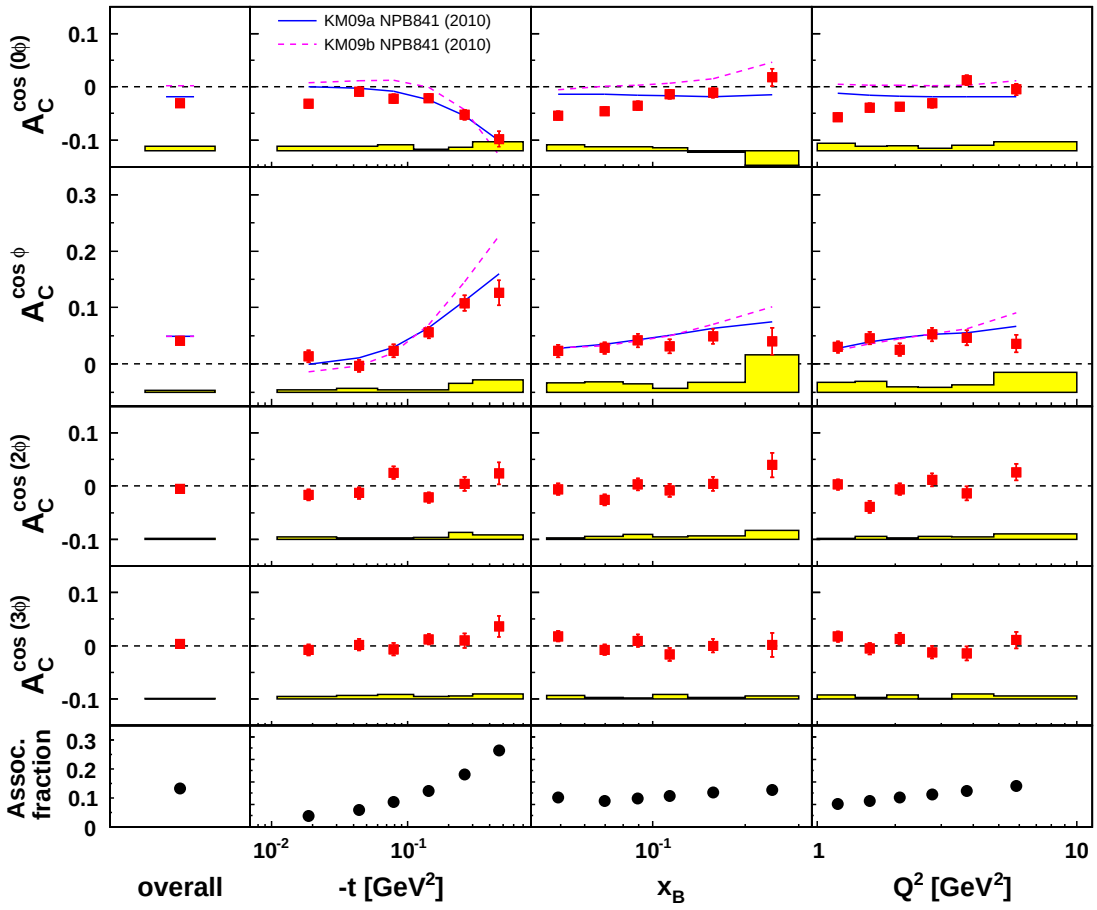

Fig. 5. The $A_C^{\cos(0\phi)}$, $A_C^{\cos\phi}$, $A_C^{\cos(2\phi)}$ and $A_C^{\cos(3\phi)}$ beam-charge amplitudes extracted from all the hydrogen data recorded at HERMES from 1996 until 2007. The error bars (bands) represent the statistical (systematic) uncertainties. Theoretical calculations from the model described in [?] are shown as solid and dashed lines. See text for details. The simulated fractional contribution from associated production to the yield in each kinematic bin is shown in the bottom row.

physically-motivated Regge dependence. The solid curves represent the model fit without data from the experiment [?] at Hall A in Jefferson Laboratory; the model fit represented by the dashed curves incorporates this data in the fit for an extraction of the GPDs. Both fits include the 1996-2005 HERMES data. The model incorporates only twist-2 GPDs and so can provide calculations only for the $A_{LU,I}^{\sin\phi}$, $A_C^{\cos(0\phi)}$ and $A_C^{\cos\phi}$ asymmetry amplitudes. The $A_{LU,I}^{\sin\phi}$ amplitude is well described by the model. Both the $A_C^{\cos(0\phi)}$ and $A_C^{\cos\phi}$ amplitudes favour the GPD fit that did not include the Hall A data.

The asymmetry amplitudes shown in Figs. 2 and 3 were also re-binned as a function of $-t$ for three different ranges of x_B. There was no observed dependence of any of the amplitudes with this two dimensional binning.

6 Summary

Beam helicity and beam charge asymmetries in the azimuthal distribution of real photons from leptoproduction on an unpolarised hydrogen target have been presented. These asymmetries were extracted from a new unpolarised hydrogen data set taken during the 2006 and 2007 operating period of HERMES. This new data set is larger than the previously publised 1996-2005 data set Ref. [**?**].

A comparison of the amplitudes extracted from these independent data sets have shown that they are compatible and asymmetry amplitudes can therefore be extracted from the complete 1996-2007 DVCS/BH event sample. The resulting asymmetry amplitudes represent the most statistically precise DVCS result that will be published by the HERMES collaboration. The result of this simultaneous extraction of asymmetry amplitudes show that there is a strong signal in the first harmonic of the interference contribution to the beam helicity asymmetry. There are also non zero amplitudes in the zeroth and first harmonic of the beam charge asymmetry. Each of the other higher order asymmetry amplitudes are consistent with zero. The combined results are compared to calculations from ongoing work to fit GPD models to experimental data. These model fits all include the HERMES data set from 1996-2005. One fitted model achieve good agreement with the presented beam-helicity asymmetry amplitude results, and fair agreement with the beam-charge asymmetry amplitudes. One leading-twist model shows good agreement with the asymmetry amplitudes that it can be used to calculate.

A Tables of Results

Kinematc Bin	$-t$ [GeV^2]	x_B	Q^2 [GeV^2]	$A_{LU,I}^{sin\phi}$ $\pm\delta_{stat.}$ $\pm\delta_{syst.}$	$A_{LU,DVCS}^{sin\phi}$ $\pm\delta_{stat.}$ $\pm\delta_{syst.}$	$A_{LU,I}^{sin(2\phi)}$ $\pm\delta_{stat.}$ $\pm\delta_{syst.}$
Overall	0.117	0.097	2.521	-0.209 ± 0.026 ± 0.026	-0.015 ± 0.026 ± 0.008	0.005 ± 0.025 ± 0.005
$0.00 \leqslant -t \leqslant 0.03$	0.018	0.068	1.720	-0.242 ± 0.055 ± 0.015	0.032 ± 0.055 ± 0.004	0.023 ± 0.055 ± 0.015
$0.03 < -t \leqslant 0.06$	0.043	0.088	2.259	-0.175 ± 0.057 ± 0.030	0.091 ± 0.062 ± 0.014	0.044 ± 0.056 ± 0.005
$0.06 < -t \leqslant 0.10$	0.078	0.099	2.512	-0.220 ± 0.062 ± 0.029	-0.051 ± 0.069 ± 0.009	-0.003 ± 0.061 ± 0.008
$0.10 < -t \leqslant 0.20$	0.142	0.110	2.785	-0.200 ± 0.054 ± 0.027	0.020 ± 0.058 ± 0.018	0.004 ± 0.054 ± 0.009
$0.20 < -t \leqslant 0.35$	0.260	0.121	3.272	-0.242 ± 0.062 ± 0.016	0.126 ± 0.079 ± 0.016	-0.073 ± 0.064 ± 0.016
$0.35 < -t \leqslant 0.70$	0.460	0.125	3.819	-0.156 ± 0.111 ± 0.023	-0.101 ± 0.114 ± 0.011	-0.119 ± 0.102 ± 0.024
$0.03 \leqslant x_B \leqslant 0.06$	0.095	0.049	1.338	-0.173 ± 0.056 ± 0.093	-0.051 ± 0.056 ± 0.018	-0.039 ± 0.056 ± 0.022
$0.06 < x_B \leqslant 0.08$	0.091	0.069	1.799	-0.260 ± 0.055 ± 0.065	0.023 ± 0.055 ± 0.003	0.042 ± 0.055 ± 0.007
$0.08 < x_B \leqslant 0.10$	0.104	0.089	2.300	-0.303 ± 0.062 ± 0.057	0.069 ± 0.062 ± 0.003	0.020 ± 0.062 ± 0.005
$0.10 < x_B \leqslant 0.13$	0.121	0.113	2.928	-0.209 ± 0.065 ± 0.043	-0.012 ± 0.065 ± 0.002	-0.007 ± 0.065 ± 0.002
$0.13 < x_B \leqslant 0.20$	0.159	0.157	4.058	-0.133 ± 0.071 ± 0.042	-0.071 ± 0.071 ± 0.025	0.018 ± 0.069 ± 0.021
$0.20 < x_B \leqslant 0.35$	0.231	0.244	6.139	-0.214 ± 0.121 ± 0.062	-0.074 ± 0.120 ± 0.024	0.021 ± 0.113 ± 0.023
$1.00 \leqslant Q^2 \leqslant 1.40$	0.076	0.054	1.199	-0.168 ± 0.055 ± 0.071	-0.037 ± 0.055 ± 0.008	-0.011 ± 0.055 ± 0.025
$1.40 < Q^2 \leqslant 1.80$	0.089	0.069	1.590	-0.282 ± 0.061 ± 0.076	0.020 ± 0.061 ± 0.018	-0.035 ± 0.060 ± 0.014
$1.80 < Q^2 \leqslant 2.40$	0.104	0.085	2.079	-0.286 ± 0.058 ± 0.067	0.082 ± 0.058 ± 0.017	0.040 ± 0.058 ± 0.004
$2.40 < Q^2 \leqslant 3.20$	0.126	0.105	2.768	-0.194 ± 0.063 ± 0.048	-0.015 ± 0.063 ± 0.012	0.038 ± 0.049 ± 0.012
$3.20 < Q^2 \leqslant 4.50$	0.151	0.134	3.764	-0.120 ± 0.047 ± 0.053	-0.119 ± 0.047 ± 0.021	-0.033 ± 0.069 ± 0.016
$4.50 < Q^2 \leqslant 10.0$	0.218	0.200	5.819	-0.178 ± 0.080 ± 0.032	-0.052 ± 0.080 ± 0.010	0.031 ± 0.076± 0.012

Table A.1
Results of the extraction of $A_{LU}^{sin(n\phi)}$ amplitudes with statistical and systematic uncertainties and average kinematics from unpolarised Hydrogen taken during the 2006-2007 experimental data taking period at HERMES for each $-t$, x_B and Q^2 bin. An additional 3.4 % scale uncertainty is present in the amplitudes due to the precision of the beam polarisation measurement.

Kinematic Bin	$-t$ [GeV^2]	x_B	Q^2 [GeV^2]	$A_C^{cos(0\phi)}$ $\pm\delta_{stat.}$ $\pm\delta_{syst.}$	$A_C^{cos\phi}$ $\pm\delta_{stat.}$ $\pm\delta_{syst.}$	$A_C^{cos(2\phi)}$ $\pm\delta_{stat.}$ $\pm\delta_{syst.}$	$A_C^{cos(3\phi)}$ $\pm\delta_{stat.}$ $\pm\delta_{syst.}$
Overall	0.117	0.097	2.521	-0.039 ± 0.004 ± 0.008	0.032 ± 0.006 ± 0.003	-0.007 ± 0.006 ± 0.002	0.009 ± 0.006 ± 0.001
$0.00 \leqslant -t \leqslant 0.03$	0.018	0.068	1.720	-0.038 ± 0.009 ± 0.007	0.015 ± 0.013 ± 0.003	-0.026 ± 0.012 ± 0.004	-0.015 ± 0.012 ± 0.003
$0.03 < -t \leqslant 0.06$	0.043	0.088	2.259	-0.013 ± 0.010 ± 0.008	-0.004 ± 0.013 ± 0.008	-0.023 ± 0.013 ± 0.003	0.000 ± 0.012 ± 0.007
$0.06 < -t \leqslant 0.10$	0.078	0.099	2.512	-0.040 ± 0.010 ± 0.011	0.027 ± 0.014 ± 0.006	0.030 ± 0.013 ± 0.005	-0.001 ± 0.013 ± 0.010
$0.10 < -t \leqslant 0.20$	0.142	0.110	2.785	-0.023 ± 0.009 ± 0.007	0.044 ± 0.012 ± 0.005	-0.016 ± 0.012 ± 0.007	0.031 ± 0.012 ± 0.004
$0.20 < -t \leqslant 0.35$	0.260	0.121	3.272	-0.058 ± 0.012 ± 0.008	0.078 ± 0.017 ± 0.015	0.008 ± 0.016 ± 0.012	0.021 ± 0.016 ± 0.005
$0.35 < -t \leqslant 0.70$	0.460	0.125	3.819	-0.130 ± 0.017 ± 0.012	0.051 ± 0.025 ± 0.004	0.015 ± 0.023 ± 0.009	0.040 ± 0.022 ± 0.009
$0.03 \leqslant x_B \leqslant 0.06$	0.095	0.049	1.338	-0.074 ± 0.010 ± 0.011	0.017 ± 0.015 ± 0.014	-0.011 ± 0.013 ± 0.002	0.003 ± 0.012 ± 0.007
$0.06 < x_B \leqslant 0.08$	0.091	0.069	1.799	-0.084 ± 0.009 ± 0.008	0.028 ± 0.012 ± 0.019	-0.010 ± 0.012 ± 0.003	0.005 ± 0.012 ± 0.004
$0.08 < x_B \leqslant 0.10$	0.104	0.089	2.300	-0.055 ± 0.010 ± 0.009	0.029 ± 0.015 ± 0.014	-0.015 ± 0.014 ± 0.007	0.014 ± 0.014 ± 0.004
$0.10 < x_B \leqslant 0.13$	0.121	0.113	2.928	-0.060 ± 0.011 ± 0.005	0.045 ± 0.015 ± 0.002	-0.031 ± 0.014 ± 0.003	-0.010 ± 0.014 ± 0.005
$0.13 < x_B \leqslant 0.20$	0.159	0.157	4.058	-0.045 ± 0.012 ± 0.003	0.036 ± 0.017 ± 0.017	0.003 ± 0.015 ± 0.006	0.010 ± 0.015 ± 0.004
$0.20 < x_B \leqslant 0.35$	0.231	0.244	6.139	0.031 ± 0.020 ± 0.028	0.059 ± 0.029 ± 0.068	0.052 ± 0.027 ± 0.018	0.050 ± 0.026 ± 0.008
$1.00 \leqslant Q^2 \leqslant 1.40$	0.076	0.054	1.199	-0.058 ± 0.009 ± 0.015	0.024 ± 0.012 ± 0.016	-0.026 ± 0.012 ± 0.004	0.0027 ± 0.012 ± 0.005
$1.40 < Q^2 \leqslant 1.80$	0.089	0.069	1.590	-0.043 ± 0.010 ± 0.008	0.038 ± 0.014 ± 0.020	-0.023 ± 0.013 ± 0.008	0.001 ± 0.013 ± 0.003
$1.80 < Q^2 \leqslant 2.40$	0.104	0.085	2.079	-0.052 ± 0.010 ± 0.007	0.007 ± 0.014 ± 0.010	0.030 ± 0.013 ± 0.001	0.043 ± 0.013 ± 0.005
$2.40 < Q^2 \leqslant 3.20$	0.126	0.105	2.768	-0.035 ± 0.011 ± 0.004	0.055 ± 0.015 ± 0.007	-0.016 ± 0.012 ± 0.004	-0.027 ± 0.014 ± 0.003
$3.20 < Q^2 \leqslant 4.50$	0.151	0.134	3.764	0.003 ± 0.012 ± 0.010	0.024 ± 0.017 ± 0.014	-0.008 ± 0.016 ± 0.003	0.015 ± 0.01 ± 0.009
$4.50 < Q^2 \leqslant 10.0$	0.218	0.200	5.819	-0.019 ± 0.014 ± 0.015	0.035 ± 0.019 ± 0.033	0.015 ± 0.023 ± 0.014	0.018 ± 0.018 ± 0.004

Table A.2
Results of the extraction of $A_C^{cos\phi}$ amplitudes with statistical and systematic uncertainties and average kinematics from unpolarised Hydrogen taken during the 2006-2007 experimental data taking period at HERMES for each $-t$, x_B and Q^2 bin.

Kinematc Bin	$-t$ [GeV^2]	x_B	Q^2 [GeV^2]	$A_{LU,I}^{sin\phi}$ $\pm\delta_{stat.}$ $\pm\delta_{syst.}$	$A_{LU,DVCS}^{sin\phi}$ $\pm\delta_{stat.}$ $\pm\delta_{syst.}$	$A_{LU,I}^{sin(2\phi)}$ $\pm\delta_{stat.}$ $\pm\delta_{syst.}$
Overall	0.118	0.097	2.505	-0.213 ± 0.020 ± 0.024	0.005 ± 0.020 ± 0.007	0.006 ± 0.020 ± 0.004
$0.00 \leqslant -t \leqslant 0.03$	0.019	0.069	1.722	-0.237 ± 0.044 ± 0.013	0.049 ± 0.044 ± 0.005	0.033 ± 0.044 ± 0.013
$0.03 < -t \leqslant 0.06$	0.044	0.088	2.245	-0.190 ± 0.045 ± 0.026	-0.023 ± 0.045 ± 0.013	0.021 ± 0.044 ± 0.007
$0.06 < -t \leqslant 0.10$	0.079	0.099	2.493	-0.213 ± 0.049 ± 0.023	-0.056 ± 0.049 ± 0.009	0.019 ± 0.048 ± 0.008
$0.10 < -t \leqslant 0.20$	0.143	0.109	2.759	-0.214 ± 0.043 ± 0.023	0.031 ± 0.042 ± 0.015	0.016 ± 0.043 ± 0.010
$0.20 < -t \leqslant 0.35$	0.261	0.119	3.232	-0.246 ± 0.055 ± 0.015	0.065 ± 0.055 ± 0.016	-0.071 ± 0.051 ± 0.015
$0.35 < -t \leqslant 0.70$	0.463	0.122	3.727	-0.157 ± 0.080 ± 0.020	-0.106 ± 0.079 ± 0.011	-0.141 ± 0.081 ± 0.024
$0.03 \leqslant x_B \leqslant 0.06$	0.099	0.049	1.343	-0.193 ± 0.044 ± 0.086	-0.013 ± 0.044 ± 0.016	-0.036 ± 0.044 ± 0.018
$0.06 < x_B \leqslant 0.08$	0.093	0.070	1.794	-0.241 ± 0.043 ± 0.057	0.023 ± 0.044 ± 0.004	0.033 ± 0.043 ± 0.006
$0.08 < x_B \leqslant 0.10$	0.106	0.089	2.303	-0.279 ± 0.049 ± 0.047	0.057 ± 0.049 ± 0.006	0.027 ± 0.049 ± 0.009
$0.10 < x_B \leqslant 0.13$	0.122	0.114	2.936	-0.219 ± 0.051 ± 0.040	-0.00 ± 0.051 ± 0.006	-0.016 ± 0.052 ± 0.004
$0.13 < x_B \leqslant 0.20$	0.160	0.157	4.062	-0.163 ± 0.056 ± 0.037	-0.043 ± 0.055 ± 0.023	-0.049 ± 0.055 ± 0.018
$0.20 < x_B \leqslant 0.35$	0.233	0.244	6.126	-0.167 ± 0.096 ± 0.047	-0.107 ± 0.091 ± 0.030	-0.022 ± 0.090 ± 0.023
$1.00 \leqslant Q^2 \leqslant 1.40$	0.078	0.055	1.199	-0.190 ± 0.043 ± 0.067	-0.007 ± 0.043 ± 0.009	-0.018 ± 0.043 ± 0.020
$1.40 < Q^2 \leqslant 1.80$	0.092	0.069	1.590	-0.247 ± 0.048 ± 0.067	0.024 ± 0.048 ± 0.018	-0.014 ± 0.047 ± 0.011
$1.80 < Q^2 \leqslant 2.40$	0.106	0.085	2.079	-0.271 ± 0.046 ± 0.057	0.074 ± 0.046 ± 0.016	0.016 ± 0.046 ± 0.005
$2.40 < Q^2 \leqslant 3.20$	0.127	0.105	2.768	-0.257 ± 0.049 ± 0.046	0.046 ± 0.049 ± 0.013	0.037 ± 0.041 ± 0.012
$3.20 < Q^2 \leqslant 4.50$	0.152	0.134	3.766	-0.115 ± 0.040 ± 0.050	-0.113 ± 0.040 ± 0.019	-0.055 ± 0.054 ± 0.012
$4.50 < Q^2 \leqslant 10.0$	0.220	0.199	5.789	-0.164 ± 0.064 ± 0.026	-0.071 ± 0.063 ± 0.011	-0.021 ± 0.061 ± 0.011

Table A.3
Results of the combination of the $A_{LU}^{sin(n\phi)}$ amplitudes with statistical and systematic uncertainties and average kinematics from unpolarised Hydrogen taken during the 1996-2007 experimental data taking period at HERMES for each $-t$, x_B and Q^2 bin. An additional 3.2 % scale uncertainty is present in the amplitudes due to the precision of the beam polarisation measurement.

Kinematc Bin	$-t$ [GeV^2]	x_B	Q^2 [GeV^2]	$A_C^{cos(0\phi)}$ $\pm\delta_{stat.}$ $\pm\delta_{syst.}$	$A_C^{cos\phi}$ $\pm\delta_{stat.}$ $\pm\delta_{syst.}$	$A_C^{cos(2\phi)}$ $\pm\delta_{stat.}$ $\pm\delta_{syst.}$	$A_C^{cos(3\phi)}$ $\pm\delta_{stat.}$ $\pm\delta_{syst.}$
Overall	0.117	0.097	2.521	-0.034 ± 0.004 ± 0.008	0.038 ± 0.005 ± 0.003	-0.006 ± 0.005 ± 0.002	0.005 ± 0.005 ± 0.001
$0.00 \leqslant -t \leqslant 0.03$	0.018	0.068	1.720	-0.035 ± 0.008 ± 0.008	0.016 ± 0.011 ± 0.003	-0.017 ± 0.011 ± 0.005	-0.008 ± 0.011 ± 0.003
$0.03 < -t \leqslant 0.06$	0.043	0.088	2.259	-0.009 ± 0.008 ± 0.007	-0.004 ± 0.011 ± 0.007	-0.018 ± 0.011 ± 0.006	0.001 ± 0.011 ± 0.006
$0.06 < -t \leqslant 0.10$	0.078	0.099	2.512	-0.028 ± 0.008 ± 0.011	0.025 ± 0.012 ± 0.007	0.028 ± 0.012 ± 0.007	-0.004 ± 0.012 ± 0.009
$0.10 < -t \leqslant 0.20$	0.142	0.110	2.785	-0.021 ± 0.007 ± 0.009	0.051 ± 0.010 ± 0.007	-0.022 ± 0.010 ± 0.011	0.018 ± 0.009 ± 0.004
$0.20 < -t \leqslant 0.35$	0.260	0.121	3.272	-0.052 ± 0.010 ± 0.007	0.100 ± 0.014 ± 0.016	-0.001 ± 0.013 ± 0.020	0.014 ± 0.013 ± 0.008
$0.35 < -t \leqslant 0.70$	0.460	0.125	3.819	-0.110 ± 0.015 ± 0.011	0.101 ± 0.022 ± 0.017	0.022 ± 0.020 ± 0.014	0.039 ± 0.019 ± 0.012
$0.03 \leqslant x_B \leqslant 0.06$	0.095	0.049	1.338	-0.066 ± 0.008 ± 0.012	0.022 ± 0.012 ± 0.013	-0.007 ± 0.011 ± 0.004	0.013 ± 0.010 ± 0.006
$0.06 < x_B \leqslant 0.08$	0.091	0.069	1.799	-0.065 ± 0.007 ± 0.008	0.032 ± 0.010 ± 0.017	-0.020 ± 0.010 ± 0.008	-0.003 ± 0.010 ± 0.003
$0.08 < x_B \leqslant 0.10$	0.104	0.089	2.300	-0.053 ± 0.009 ± 0.010	0.039 ± 0.012 ± 0.017	-0.002 ± 0.012 ± 0.010	0.009 ± 0.012 ± 0.006
$0.10 < x_B \leqslant 0.13$	0.121	0.113	2.928	-0.041 ± 0.009 ± 0.006	0.037 ± 0.013 ± 0.021	-0.016 ± 0.012 ± 0.004	-0.017 ± 0.012 ± 0.005
$0.13 < x_B \leqslant 0.20$	0.159	0.157	4.058	-0.036 ± 0.010 ± 0.006	0.050 ± 0.014 ± 0.021	0.004 ± 0.013 ± 0.005	0.006 ± 0.013 ± 0.005
$0.20 < x_B \leqslant 0.35$	0.231	0.244	6.139	-0.012 ± 0.017 ± 0.028	0.054 ± 0.024 ± 0.053	0.042 ± 0.023 ± 0.020	0.015 ± 0.023 ± 0.001
$1.00 \leqslant Q^2 \leqslant 1.40$	0.076	0.054	1.199	-0.054 ± 0.007 ± 0.016	0.031 ± 0.010 ± 0.020	0.014 ± 0.010 ± 0.006	0.014 ± 0.010 ± 0.005
$1.40 < Q^2 \leqslant 1.80$	0.089	0.069	1.590	-0.040 ± 0.008 ± 0.011	0.045 ± 0.012 ± 0.018	-0.007 ± 0.011 ± 0.010	-0.007 ± 0.011 ± 0.003
$1.80 < Q^2 \leqslant 2.40$	0.104	0.085	2.079	-0.041 ± 0.008 ± 0.009	0.018 ± 0.011 ± 0.011	0.025 ± 0.011 ± 0.002	0.025 ± 0.011 ± 0.006
$2.40 < Q^2 \leqslant 3.20$	0.126	0.105	2.768	-0.032 ± 0.008 ± 0.005	0.054 ± 0.013 ± 0.007	-0.020 ± 0.012 ± 0.008	-0.020 ± 0.012 ± 0.006
$3.20 < Q^2 \leqslant 4.50$	0.151	0.134	3.764	0.008 ± 0.009 ± 0.010	0.031 ± 0.014 ± 0.011	-0.003 ± 0.013 ± 0.007	-0.003 ± 0.013 ± 0.006
$4.50 < Q^2 \leqslant 10.0$	0.218	0.200	5.819	-0.014 ± 0.010 ± 0.014	0.040 ± 0.016 ± 0.039	0.013 ± 0.015 ± 0.012	0.013 ± 0.015 ± 0.005

Table A.4
Results of the combination of the $A_C^{cos\phi}$ amplitudes with statistical and systematic uncertainties and average kinematics from unpolarised Hydrogen taken during the 1996-2007 experimental data taking period at HERMES for each $-t$, x_B and Q^2 bin.

References

[1] D. Mueller, D. Robaschik, B. Geyer, F. M. Dittes, and J. Hoeji, "Wave Functions, Evolution Equations and Evolution Kernels from Light-Ray Operators of QCD," *Fortsch.Phys.*, vol. 42, p. 101, 1994.

[2] X. Ji, "Gauge-Invariant Decomposition of Nucleon Spin and Its Spin-Off," *Phys.Rev.Lett.*, vol. 78, pp. 610–613, 1997.

[3] A. V. Radyushkin, "Scaling Limit of Deeply Virtual Compton Scattering," *Phys.Lett. B*, vol. 380, pp. 417–425, 1996.

[4] The HERMES Collaboration, A. Airapetian et al., "Separation of contributions from deeply virtual Compton scattering and its interference with the Bethe–Heitler process in measurements on a hydrogen target," *JHEP*, vol. 0911, p. 083, Sept. 2009.

[5] The HERMES Collaboration, A. Airapetian et al., "Measurement of azimuthal asymmetries associated with deeply virtual Compton scattering on an unpolarized deuterium target," *Nucl. Phys.*, vol. B 829, pp. 1–27, Nov. 2009.

[6] The HERMES Collaboration, A. Airapetian et al., "The Beam–Charge Azimuthal Asymmetry and Deeply Virtual Compton Scattering," *Phys.Rev.D*, vol. 75:011103, 2007.

[7] The HERMES Collaboration, A. Airapetian et al., "Exclusive leptoproduction of real photons on a longitudinally polarised hydrogen target," *JHEP 06*, vol. 019, 2010.

[8] The HERMES Collaboration, A. Airapetian et al., "Measurement of the Beam-Spin Azimuthal Asymmetry Associated with Deeply-Virtual Compton Scattering," *Phys.Rev.Lett.*, vol. 87, p. 182001, 2001.

[9] A. V. Belitsky, D. Mller, and A. Kirchner, "Theory of deeply virtual Compton scattering on the nucleon," *Nucl.Phys. B*, vol. 629, pp. 323–392, 2002.

[10] K. Ackerstaff, "The HERMES Spectrometer," *Nucl.Instrum.Meth. A*, vol. 417, pp. 230–265, 1998.

[11] T. Benisch et al., "The luminosity monitor of the HERMES experiment at DESY," *Nucl. Instrum. Meth. A.*, vol. 471, pp. 314–324, 2001.

[12] J. Burns, *Deeply Virtual Compton Scattering off an Unpolarised Hydrogen Target at HERMES.* PhD thesis, University of Glasgow, 2010.

[13] D. Zeiler, *Deeply Virtual Compton Scattering off an Unpolarized Hydrogen Target at the HERMES Experiment.* PhD thesis, University Erlangen-Nuremberg, 2009.

[14] R. Barlow, "Extended Maximum Likelihood," *Nucl. Instrum. Meth. A.*, vol. 297, pp. 496–506, 1990.

[15] The HERMES Collaboration, A. Airapetian et al., "Measurement of Azimuthal Asymmetries With Respect To Both Beam Charge and Transverse Target Polarization in Exclusive Electroproduction of Real Photons," *JHEP*, vol. 06, p. 066, Feb. 2008.

[16] F. Brasse et al. *Nucl. Phys. B*, vol. 110, p. 413, 1976.

[17] V. Guzey and T. Teckentrup, "The dual parameterization of the proton generalized parton distribution functions H and E and description of the DVCS cross sections and asymmetries," *Phys.Rev. D*, vol. 74:054027, 2006.

[18] K. Kumericki and D.Mueller, "Deeply virtual Compton scattering at small x_B and the access to GPD H." arXiv:0904.0458.

[19] F. X. Girod and R. A. Niyazov et al, "Deeply Virtual Compton Scattering Beam-Spin Asymmetries," *Phys.Rev.Lett.*, vol. 100, p. 162002, Nov. 2008.